Theor Chem Acc (2011) 128:769–782
DOI 10.1007/s00214-010-0832-5

REGULAR ARTICLE

Vibrational dynamics of polyatomic molecules in solution: assignment, time evolution and mixing of instantaneous normal modes

Adrián Kalstein · Sebastián Fernández-Alberti · Adolfo Bastida · Miguel Angel Soler · Marwa H. Farag · José Zúñiga · Alberto Requena

Received: 29 June 2010 / Accepted: 24 September 2010 / Published online: 13 October 2010

Abstract Intramolecular vibrational dynamics of polyatomic molecules in solution can be addressed through normal mode analysis based on either equilibrium normal modes (ENMs) or instantaneous normal modes (INMs). While the former offers a straightforward way of examining experimental spectra, the latter provides a decoupled short-time description of the vibrational motions of the molecule. In order to reconcile both representations, a realistic assignment of the INMs in terms of the ENMs is needed. In this paper, we describe a novel method to assign the INMs using the ENMs as templates, which provides a unique relationship between the two sets of normal modes. The method is based specifically on the use of the so-called Min-Cost or Min-Sum algorithm, duly adapted to our problem, to maximize the overlaps between the two sets of modes. The identification of the INMs as the system evolves with time then allows us to quantify the vibrational energy stored in each INM and so monitor the flows of intramolecular vibrational energy within the solute molecule. We also discuss the degree of mixing of the INMs and characterize the way they change with time by means of the corresponding autocorrelation functions. The usefulness of the method is illustrated by carrying out equilibrium molecular dynamics (MD) simulations of the deuterated *N*-methylacetamide (NMAD) molecule in D_2O solution.

Keywords Equilibrium normal modes · Instantaneous normal modes · Vibrational energy relaxation · Biomolecules in solution

1 Introduction

Understanding the vibrational motions of a polyatomic molecule in solution is critical in describing the intramolecular energy redistribution and intermolecular energy transfer processes that take place during the vibrational relaxation of the solute molecule. Recent advances in ultrafast infrared–Raman techniques have been shown to provide a remarkably detailed description of the vibrational energy flows throughout polyatomic molecules in liquids [1–13]. Transient spectroscopic data give quantitative measures of the instantaneous populations of all the observed vibrations of the molecule in real time. The information extracted from these experiments is usually discussed in terms of the vibrational spectra assigned using the standard equilibrium normal modes (ENM). However, since the definition of these modes is based on the second-order expansion of the potential energy function of the isolated solute molecule about its equilibrium configuration, their ability to describe the intramolecular vibrational dynamics of the molecule in aqueous solution at room temperature in terms of individual normal modes seems to be questionable [14].

Structural perturbations caused by the interaction of the solute molecule with the solvent and by the effect of the thermal energy stored in the molecule produce, in fact, large conformational changes driven by the vibrational

Published as part of the special issue celebrating theoretical and computational chemistry in Spain.

A. Kalstein · S. Fernández-Alberti
Universidad Nacional de Quilmes,
Roque Saenz Peña 352, B1876BXD Bernal, Argentine

A. Bastida (✉) · M. A. Soler · M. H. Farag · J. Zúñiga · A. Requena
Departamento de Química Física,
Universidad de Murcia, 30100 Murcia, Spain
e-mail: bastida@um.es

dynamics anharmonicities. This behavior is particularly well known in biomolecules, where rugged energy landscapes indicate the presence of a very large number of nearly isoenergetic conformations, which are accessible in solution at room conditions [15–18]. Mode couplings have indeed been revealed as a basic requirement to describe the vibrational energy transfer and vibrational absorption spectra of proteins [19, 20]. The effect of anharmonic motions in the vibrational dynamics of macromolecules has also been extensively studied by Go and co-workers [21–23], who use the ENMs and conclude that while high-frequency ENMs preserve significant harmonic aspects, low-frequency modes remain essentially anharmonic.

The inherent structures of large systems can be determined through molecular dynamics simulations by quenching the instantaneous structures to local minima of the potential energy surface. The so-called Quenched Normal Modes (QNMs) [24–29] can be therefore calculated by diagonalization of the corresponding Hessian matrices. Furthermore, QNMs can be evaluated for super molecules, including the solute molecule and its first solvation shell. However, the QNMs do not provide an expression for the vibrational energy of the molecule as a sum of individual contributions from every single mode at the instantaneous configurations of the solute molecule. We also note that the presence of the solvent can increase the number of conformers, each with a different set of QNMs, significantly. Another approach to deal with the vibrational dynamics, which is far from the equilibrium configuration, consists of calculating effective quadratic force constants by averaging on the potential of mean force at a given temperature. This method is called the quasi-harmonic approximation [30–32], and although it can deal with the effective force constants as a function of temperature, its application to nonequilibrium molecular dynamics simulations is not straightforward.

The strong couplings emerging between the ENMs of the solute molecule when it executes wide amplitude vibrational motions severely complicate the interpretation of the vibrational dynamics of the molecule in terms of individual contributions of each mode. The same happens with the vibrational energy flows, which cannot therefore be quantified in terms of the energy stored in each individual ENM. Achieving this is, however, essential to describe the evolution with time of the excess of vibrational energy deposited in a given mode, both for the understanding of the process and above all because this energy can now be experimentally tracked by ultrafast infrared–Raman spectroscopy, thus making direct comparison with the experiment possible. One way to tackle this problem is to use the instantaneous normal modes (INMs), which are those obtained by diagonalizing the Hessian matrix of the potential energy function at every instantaneous configuration of the molecule. The INM theory was originally developed to study short-time dynamics properties of liquids [33–44], where it is shown to provide a conceptually and computationally simple harmonic picture of the system, and it has been extended later to study the vibrational dynamics of polyatomic molecules in solution [14, 26, 29, 45, 46–49], thus widening its range of applications.

The INM formalism is based on the fact that, at any instant, intramolecular vibrations closely resemble a set of well-defined and independent harmonic oscillators. Accordingly, the INMs change as the configuration of the molecule evolves with time, and this INMs evolution can be related to time-resolved spectroscopic observables. In this respect, for instance, time correlation functions obtained using INMs have been calculated and tested for a variety of atomic and molecular liquids [34, 50–56]. Clearly, a single set of INMs cannot represent the long-time dynamics of the solute molecule, since its validity is limited to the vicinity of the configuration from which the set has been extracted. It is necessary then to compute successive sets of INMs of the evolving molecule from molecular dynamics simulations and find a meaningful way to connect them, and this requires in turn an efficient method to assign and, therefore, identify the individual INMs .

The simplest way to identify the INMs with time is to sort them by increasing frequencies, provided that the INMs are calculated at time steps short enough to get a smooth variation. Even in this case, however, the identification of the INMs based on their history poses some difficulties that make it impractical [36]. These difficulties arise basically from the fact that the time-dependent vibrational frequencies of the INMs may become very close and even cross with either significant or no effects on the INM definitions, thus complicating their identification severely. Accordingly, a more efficient method of identification of the INMs with time must be devised based on the specific assignments of the INMs at every time step of the MD simulation.

In this paper, we extensively develop a novel method previously proposed by our group [48, 49] to track the identity of the INMs over time, which is based on the use of the ENMs as templates to assign the INMs at a given time. The method therefore reconciles the descriptions of the vibrational dynamics based on both sets of modes and provides, in addition, a unique relationship between them. To illustrate the method, we perform equilibrium MD simulations of the deuterated *N*-methylacetamide (NMAD) molecule in D_2O solution. The choice of this system is guided by the large number of experimental [2, 3, 13, 57–62] and theoretical [14, 29, 46, 59, 63–68] studies that it has received and which validate the NMAD molecule as a simple model for the amide bond in peptides and proteins. The paper is then organized as follows. In Sect. 2, we review the fundamental

aspects of the INM methodology, present the algorithm proposed to identify them, and give the computational details of the MD simulations carried out for the NMAD/D_2O(l) system. Section 3 is devoted to discussing the results obtained from the application of the INM identification method to the NMAD/D_2O(l) system and finally the summary and the conclusions are given in Sect. 4.

2 Methodology

2.1 Instantaneous normal mode formalism

For a given polyatomic solute molecule in a solvent bath, the total energy of the system can be written as follows

$$E_{\mathrm{tot}} = E_{\mathrm{S}} + E_{\mathrm{B}} + V_{\mathrm{I}} \tag{1}$$

where E_{S} and E_{B} are the energies depending, respectively, on the solute and bath coordinates and V_{I} is the interaction energy. By neglecting the rotational-vibrational couplings of the solute molecule [46], its energy E_{S} can be expressed in turn in the form

$$E_{\mathrm{S}} = E_{\mathrm{S}}^{\mathrm{trans}} + E_{\mathrm{S}}^{\mathrm{rot}} + E_{\mathrm{S}}^{\mathrm{vib}} \tag{2}$$

where $E_{\mathrm{S}}^{\mathrm{trans}}, E_{\mathrm{S}}^{\mathrm{rot}}$, and $E_{\mathrm{S}}^{\mathrm{vib}}$ are the translational, rotational, and vibrational energies of the solute, respectively.

Let us focus our attention on the vibrational energy of solute $E_{\mathrm{S}}^{\mathrm{vib}}$. Using the standard equilibrium normal coordinates $\boldsymbol{Q}^{\mathrm{e}} = (Q_1^{\mathrm{e}}, \ldots, Q_N^{\mathrm{e}})$ to describe the vibrational motion of the molecule, we write the vibrational energy $E_{\mathrm{S}}^{\mathrm{vib}}$ as follows

$$E_{\mathrm{S}}^{\mathrm{vib}} = \frac{1}{2}\sum_{i=1}^{N}(\dot{Q}_i^{\mathrm{e}})^2 + V_{\mathrm{S}}(\boldsymbol{Q}^{\mathrm{e}}) \tag{3}$$

where N is the number of vibrational coordinates, and $V_{\mathrm{S}}(Q_i^{\mathrm{e}})$ is the intramolecular potential energy function. The ENMs are, by definition, the eigenvectors of the cartesian Hessian matrix of V_{S} evaluated at the equilibrium geometry of the solute molecule. They thus provide a decoupled harmonic description of the vibrational motions at configurations which are close to the equilibrium geometry, and the vibrational energy of the solute can be then approximated as a sum of one-mode vibrational energies as follows

$$E_{\mathrm{S}}^{\mathrm{vib}} = \sum_{i=1}^{N} E_i^{\mathrm{ENM}} \tag{4}$$

where

$$E_i^{\mathrm{ENM}} = T_i^{\mathrm{ENM}} + V_{i,\mathrm{har}}^{\mathrm{ENM}} = \frac{1}{2}(\dot{Q}_i^{\mathrm{ENM}})^2 + \frac{1}{2}\lambda_i^e(Q_i^{\mathrm{ENM}})^2 \quad i = 1, \ldots, N \tag{5}$$

and λ_i^e are the equilibrium normal force constants.

The solute molecule in solution may explore in any case configurations, which are quite far from the equilibrium geometry, with the corresponding enhancement of the vibrational couplings between the ENMs. This eventually deteriorates the separable description provided by the ENMs and rules out the use of Eq. (4) to evaluate the vibrational energy of the solute molecule in terms of the individual normal mode contributions. This problem can be addressed by introducing the INMs, which are defined as the eigenvectors of the cartesian Hessian matrix of the potential $V = V_{\mathrm{S}} + V_{\mathrm{I}}$, computed at snapshot configurations generated, for example, during Molecular Dynamics (MD) simulations of the system. These modes provide an instantaneous decoupled second-order description of the vibrational motions of the solute molecule as it evolves over time.

In the assignment of the INMs, it is convenient to express these in terms of the ENMs. To do this, we first expand the potential V in a power series of the ENMs about the instantaneous configuration of the molecule at a given time t_0, as follows

$$V = V(Q_i^{\mathrm{e}}(t_0)) + \sum_{i=1}^{N} K_i(Q_i^{\mathrm{e}} - Q_i^{\mathrm{e}}(t_0)) + \frac{1}{2}\sum_{i=1}^{N}\sum_{j=1}^{N} K_{ij}(Q_i^{\mathrm{e}} - Q_i^{\mathrm{e}}(t_0))(Q_j^{\mathrm{e}} - Q_j^{\mathrm{e}}(t_0)) + \ldots \tag{6}$$

where K_i and K_{ij} are the corresponding linear and quadratic ENM force constants. Then, in a second step, we diagonalize the resulting ENM Hessian matrix $\boldsymbol{K}$,

$$\boldsymbol{L}^{\dagger}\boldsymbol{K}\boldsymbol{L} = \lambda \tag{7}$$

in order to determine the vibrational frequencies $\nu_i = \sqrt{\lambda_i}/2\pi$ of the INMs, and the eigenvector matrix $\boldsymbol{L}$, whose elements relate the INMs with the ENMs as follows

$$Q_i^{\mathrm{INM}} = \sum_{j=1}^{N} l_{ji}(Q_j^{\mathrm{e}} - Q_j^{\mathrm{e}}(t_0)) \quad i = 1, \ldots, N \tag{8}$$

Since the $\boldsymbol{L}$ matrix is orthogonal, the inverse transformations to Eq. (8) reads

$$Q_j^{\mathrm{e}} = \sum_{i=1}^{N} l_{ji} Q_i^{\mathrm{INM}} + Q_j^{\mathrm{e}}(t_0) \quad j = 1, \ldots, N \tag{9}$$

and by differentiating this expression with respect to time, we obtain the relationship between the momenta

$$\dot{Q}_j^{e} = \sum_{i=1}^{N} l_{ji}\, \dot{Q}_i^{\mathrm{INM}} \quad i = 1, \ldots, N \tag{10}$$

Also it can be easily shown that the vibrational kinetic energy transforms in terms of the INM momenta as follows

$$T^{\mathrm{vib}} = \frac{1}{2}\sum_{i=1}^{N}(\dot{Q}_i^{\mathrm{e}})^2 = \frac{1}{2}\sum_{i=1}^{N}(\dot{Q}_i^{\mathrm{INM}})^2 \tag{11}$$

As far as the potential energy function is concerned, after substitution of Eq. (9) into Eq. (6) and proper use of Eq. (7), we get the following expression for V up to second order in terms of the INMs,

$$V = V_0 + \frac{1}{2}\sum_{i=1}^{N}\lambda_i(Q_i^{\mathrm{INM}} + a_i)^2 \tag{12}$$

where a_i are the coordinate shifts given by

$$a_i = \frac{1}{\lambda_i}\sum_{j=1}^{N}K_j l_{ji} \quad i = 1,\ldots,N \tag{13}$$

and V_0 is the shift-corrected equilibrium potential

$$V_0 = V(Q_i^{\mathrm{e}}(t_0)) - \frac{1}{2}\sum_{i=1}^{N}\lambda_i a_i^2 \tag{14}$$

The vibrational energy of the solute molecule (Eq. (3)) can be then approximated by the expression

$$E_{\mathrm{S}}^{\mathrm{vib}} = V_0 + \sum_{i=1}^{N}E_i^{\mathrm{INM}} \tag{15}$$

where

$$E_i^{\mathrm{INM}} = T_i^{\mathrm{INM}} + V_{i,\mathrm{har}}^{\mathrm{INM}} = \frac{1}{2}(\dot{Q}_i^{\mathrm{INM}})^2 + \frac{1}{2}\lambda_i(Q_i^{\mathrm{INM}} + a_i)^2 \quad i = 1,\ldots,N \tag{16}$$

The vibrational energy of the solute $E_{\mathrm{S}}^{\mathrm{vib}}$ is thus decomposed into single INM contributions, provided, as is the case, that V_0 fluctuates around a constant value [14].

2.2 Instantaneous normal modes assignment

The fact that the INMs provide a decoupled harmonic description of the vibrational motions of the solute molecule at any instantaneous configuration is fundamental to evaluate the averaged energies and populations of the vibrational modes of the molecule as a function of time and thus compare them with the observed values extracted from time-resolved infrared–Raman experiments. To achieve this, it is clear then that the INMs have to be identified as they evolve with time, and this is not a simple task since the complexity of the potential energy function of the molecule may cause them to vary substantially with time and, eventually, to mix them strongly, inducing crossings between them when some of their time-dependent frequencies come close [36]. This is essentially the reason why previous applications of the INMs have been restricted to studying short-time dynamical properties of the system [34, 50,69, 70]. In this context also, the identification of the INMs simply sorting them by increasing frequencies has been revealed to be useless [36, 48, 49].

The identification of the INMs as they evolve with time can be made by assigning them properly at each instantaneous snapshot and by using the corresponding assignment labels to connect the successive sets of INMs. The ENMs become in this respect the natural candidates to track the identity of the INMs over time [48, 49]. Accordingly, we assign the INMs at each instantaneous configuration by analyzing the relative values of l_{ij}^2 coefficients which, according to Eq. (8), measure the weight of the ith ENM in the jth INM. Depending on the contributions of the ENMs, the resulting INMs can be classified as pure or mixed [48, 49]. In a pure INM, one of the l_{ij}^2 coefficients is dominant so the INM is quite similar to the corresponding ENM. A mixed INM includes, however, significant contributions from different ENMs. The pure INMs are easy to identify at any time during the simulations and basically mimic the well-defined motions of the molecule associated with the dominant ENM. In contrast, the mixed INMs are difficult to identify due to the variations with time of their sparse ENM contributions. These modes sometimes appear as groups of modes which exchange the contributions of a given number of ENMs, displaying complicated motions of the molecule.

In our previous works [48, 49], we have shown that the assignment of the INMs based on the selection of the highest values of the corresponding l_{ij}^2 coefficients is not practical since it may give assignments of different INMs to the same ENM, which complicates the connection with the next set of INMs. To identify the INMs over time in terms of the ENMs, it is therefore necessary to establish a one-to-one correspondence between both sets of modes, and this can be done by selecting those elements of the $\boldsymbol{L}$ matrix, one for each row, and each pertaining to a different column, which maximize the sum of their squared values. This is, in fact, a variant of the well-known Min-Cost or Min-Sum assignment problem, which in general states the following: given an $N \times N$ cost matrix $\boldsymbol{C} = \{c_{ij}\}$, with $c_{ij} \geq 0$ for all i and j, assign each row to one column, and viceversa, so as to minimize the cost given by the sum of the row-column assignments. The Min-Cost assignment problem consists therefore of finding a permutation (f_i) of the integers 1,2,…,N which minimizes the trace z given by

$$z = \sum_{i=1}^{N}c_{i,f_i} \tag{17}$$

and can be efficiently solved using the so-called Hungarian algorithm [71]. For a given matrix, this algorithm then provides a set of elements, each one belonging to a different row and column, whose sum is minimal. So, in order

to maximize z, as required in our case, we apply the algorithm to the matrix of negative values of the l_{ij}^2 elements, that is, we set $c_{ij} = -l_{ij}^2$.

The direct Min-Cost assignment method of INMs has been previously used in our group to study the vibrational relaxation of the amide I mode and the CH stretchings of NMAD in D_2O solution by means of nonequilibrium MD simulations [48, 49]. In some cases, this method may lead to unphysical assignments when two or more INMs have significant contributions of some ENMs with frequencies quite apart. Reiterated crossed assignments of the INMs give place in this case to critical displacements in their averaged frequencies and to large uncertainties in their vibrational energies. This behavior supposes, then, a serious problem in monitoring the vibrational energy stored in a given mode, but can be avoided by restricting the application of the Min-Cost algorithm to ranges of frequencies of width $\Delta\omega$ centered at the ENM frequencies ω_i^e. Thus, only those INMs whose frequencies lie in the window $(\omega_i^e - \Delta\omega/2, \omega_i^e + \Delta\omega/2)$ are susceptible to being assigned to the ith ENM. In practice, this restriction is implemented by giving arbitrary high values to the corresponding $c_{ij} = -l_{ij}^2$ matrix elements, thus eliminating the possibility of them being included in the permutation which minimizes the trace given by Eq. (17). Including restrictions in the Min-Cost algorithm is expected to take away some of the efficiency of the method at maximizing the overlaps between the two sets of normal modes. The optimal choice of the frequency window width $\Delta\omega$ should compromise then the smallest as possible decrease in the averaged values of the highest l_{i,f_i}^2 coefficients relative to those obtained using the unrestricted Min-Cost algorithm ($\Delta\omega = \infty$), with the need to avoid any possible unphysical assignments of the INMs that may arise.

2.3 Molecular dynamics simulations: application to NMAD in $D_2O_{(l)}$

In order to study in depth the method proposed to assign and identify the INMs of a polyatomic molecule in solution, we have conducted MD simulations of the NMAD molecule (H_3C–COND–CH_3) in D_2O solution. The simulations are performed by placing a NMAD molecule in a cubic box of 1.975 nm length plus a number of 251 molecules of D_2O chosen to reproduce the experimental density [72] ($\rho = 1.10436$ g/cm^3). We use the AMBER force field [73] to model the solute NMAD molecule, and the flexible TIP3P water model with doubled hydrogen masses included in the CHARMM [74] force field to represent the D_2O solvent. Subroutines of the TINKER modeling package [75] are also used in our code to evaluate the forces and the potential energy function. Periodic boundary conditions are imposed to simulate the bulk system, and a cutoff of 10 Å is applied to non bonded interactions.

As in our previous works [48, 49], the coordinates used to describe the NMAD molecule motions are the center of mass vector for translations, the quaternions for rotations, and the equilibrium normal modes to propagate the vibrations. The deuterated molecules of the solvent are, in turn, described using Cartesian coordinates. The equations of motions are integrated using the leap-frog algorithm [76, 77], with a time step of 0.5 fs. The ENMs of the NMAD molecule employed are those corresponding to the optimized geometry of the *trans-cc*-NMA conformer, which is the most stable as calculated using the AMBER force field. These ENMs provide, in addition, normal modes frequencies which are in good agreement with previously reported values [63, 78, 79].

We have performed 16 *NVT* equilibrium MD simulations of 1,250 ps started using random velocities. The temperature was maintained at a mean value of 300 K by coupling to a thermal bath [80] with a time constant of 0.1 ps. The last 500 ps of these trajectories were used to collect the equilibrated configurations at 20 ps intervals. Thus, 400 sets of initial positions and momenta were stored for the subsequent non-equilibrium MD simulations, which were performed in the *NVE* ensemble in order to avoid any influence of velocity scaling on the results. Accordingly, 400 trajectories of 5 ps were propagated in order to obtain reasonable statistics for all the quantities reported. An additional set of 400 trajectories for the equilibrated NMAD molecule in vacuo were propagated to compare with the results obtained in solution.

3 Numerical results and discussion

To put the present study in perspective, we start by analyzing the ability of the ENMs to evaluate the vibrational energy of the solute molecule in terms of their individual contributions, as given by Eqs. (4) and (5). Accordingly, in Table 1 we include the averaged kinetic $\langle T_i^{\mathrm{ENM}} \rangle$ and harmonic potential $\langle V_{i,\mathrm{har}}^{\mathrm{ENM}} \rangle$ energies calculated from the equilibrium MD simulations of the NMAD molecule both in vacuo and in D_2O solution. As observed, the values of $\langle T_i^{\mathrm{ENM}} \rangle$ reproduce well, in both cases, the expected equilibrium thermodynamic value at 300 K of $k_BT/2 = 104.3$ cm^{-1}, within the standard deviations calculated of about $\pm$ 8 cm^{-1}. In contrast, most of the $\langle V_{i,\mathrm{har}}^{\mathrm{ENM}} \rangle$ values deviate in one way or another from the thermodynamic value and, as a consequence, the virial theorem, $V^{\mathrm{vib}} = T^{\mathrm{vib}}$, is not fulfiled. This behavior is due to the strong anharmonicities and couplings that emerge between the ENMs when the solute molecule explores regions of the phase space which

Table 1 Mean kinetic and harmonic potential energies (in cm^{-1}) for the ENMs and INMs of the NMAD molecule in vacuo and in D_2O solution

Mode	NMAD in vacuo				NMAD/$D_2O_{(l)}$			
	$\langle T_i^{ENM}\rangle$	$\langle V_{i,har}^{ENM}\rangle$	$\langle T_i^{INM}\rangle$	$\langle V_{i,har}^{INM}\rangle$	$\langle T_i^{ENM}\rangle$	$\langle V_{i,har}^{ENM}\rangle$	$\langle T_i^{INM}\rangle$	$\langle V_{i,har}^{INM}\rangle$
1	110.3	64.3	111.1	79.4	103.8	66.6	101.6	18.2
2	106.4	131.6	108.6	29.1	101.9	127.8	101.5	−16.3
3	105.4	96.3	107.6	454.0	101.1	94.5	101.0	−23.2
4	108.8	95.3	109.4	100.8	101.3	96.4	101.0	96.4
5	108.1	107.3	108.1	110.1	103.4	103.6	103.3	105.8
6	107.7	110.5	108.0	99.0	105.2	104.4	104.0	109.5
7	109.8	116.6	110.0	111.5	104.3	111.7	104.2	105.1
8	109.6	97.8	111.5	102.2	103.8	95.5	103.4	94.5
9	98.4	104.9	99.2	105.8	101.1	107.7	101.3	108.0
10	104.2	169.1	103.6	110.6	106.0	164.5	105.4	112.5
11	106.0	192.3	105.8	111.1	103.0	194.8	104.6	109.5
12	107.2	310.3	105.9	110.4	104.2	317.3	106.5	110.8
13	105.2	236.3	105.6	109.6	106.4	225.8	107.2	111.3
14	104.5	171.5	104.6	110.2	103.7	165.0	104.5	110.5
15	106.1	297.3	105.8	104.1	106.9	313.5	107.2	105.1
16	105.0	9,510.9	106.5	108.9	105.5	9,095.4	105.0	106.8
17	106.8	259.6	107.3	96.6	103.3	267.5	104.6	94.2
18	106.8	2,951.5	106.2	100.6	104.8	2,744.5	104.1	98.9
19	106.3	7,044.2	106.5	106.8	105.1	7,097.3	104.1	104.8
20	106.0	177.1	106.5	102.8	103.2	163.7	103.2	99.0
21	106.6	9,856.6	105.6	106.6	102.7	10,312.0	103.8	104.0
22	106.0	21,296.9	106.1	112.2	105.7	21,244.0	105.8	112.0
23	103.8	763.7	103.8	105.4	108.6	687.7	109.0	110.7
24	104.0	228.3	103.8	105.2	106.7	273.0	106.8	108.2
25	105.8	436,760.0	105.1	107.6	102.5	415,024.0	102.8	104.9
26	109.9	546,327.0	105.9	108.5	102.3	555,270.0	103.5	105.9
27	105.1	731.9	103.7	105.8	105.8	767.7	102.3	104.5
28	106.5	735.3	105.2	107.2	102.2	860.8	102.3	104.5
29	103.9	592.5	103.9	105.9	102.4	570.1	102.7	104.7
30	103.6	591.7	102.8	104.8	102.9	618.9	103.1	105.0

are far from the equilibrium one, and it clearly limits the interpretation of the vibrational energy content of the individual ENMs based on their averaged kinetic energies $\langle T_i^{ENM}\rangle$ as proposed by Raff [81, 82]. We note also that the differences between the values of $\langle V_{i,har}^{ENM}\rangle$ obtained in vacuo and in solution are smaller than their corresponding differences with the expected equilibrium $k_BT/2$ value of 104.3 cm^{-1}. This indicates that the deviations of $\langle V_{i,har}^{ENM}\rangle$ from the equilibrium value come essentially from the intramolecular contributions to $\langle V_{i,har}^{ENM}\rangle$, with only a minor influence from the intermolecular interactions with the solvent. From all this we see then that is not possible to express the vibrational energy of the solute molecule accurately, E_S^{vib}, as the sum of harmonic contributions of the ENMs. Alternatively, this can be achieved by using the INMs through Eqs. (15) and (16), as will be demonstrated below.

Let us consider the use of the INMs to analyze the vibrational dynamics of the solute. As commented above, the identification of the INMs using just the frequency order criterion is meaningless, due to the facility with which the INMs mix and cross. To see this clearer in Fig. 1, we display the evolution with time of a set of NMAD INM frequencies during a short period of time of an MD simulation. As Stratt et al. [36] have shown in pure liquid dynamics [36], a multitude of crossings or avoided crossings between the INMs frequencies seem to occur, which rule out the use of frequency ordering to identify the INMs. It is important to remark here that, while the pioneering studies of Stratt et al. [36] on liquid dynamics refer

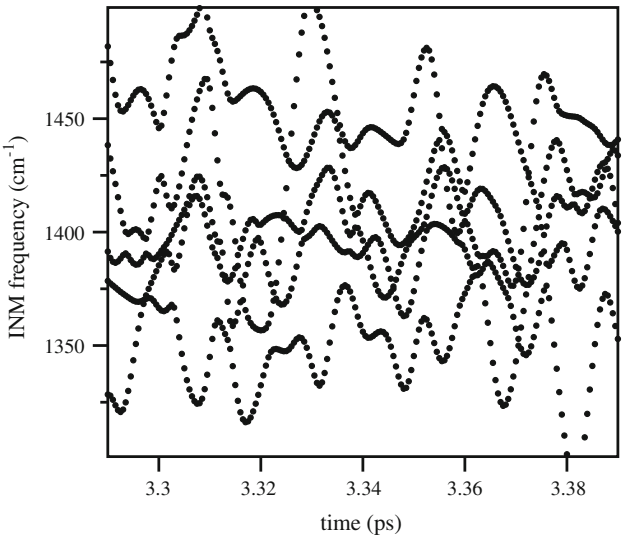

Fig. 1 Evolution with time of the INM frequencies of the NMAD molecule in a region roughly in the *middle* part of the spectrum, obtained during a short-time interval of an MD simulation of the NMAD in D_2O solution at 300 K

to INM frequencies associated with weak intermolecular potentials, our work deals with strong intramolecular potentials.

While sorting the INMs by increasing frequencies is therefore not sufficient to properly identify the INMs, the use of their corresponding l_{ij}^2 values allows us to label them according to their closeness to the ENMs. A more specific example in this respect is presented in Fig. 2 where the time-evolution of the 25th and 26th INM frequencies during a time interval in which they approach each other is shown, along with the overlap l_{ij}^2 values of these INMs with the 25th and 26th ENMs, which correspond to the NMAD C–H stretching modes ($\nu_s(CH_3)$). As observed, the variations with time of the l_{ij}^2 values indicate that the INMs exchange their identities three times in the time interval considered, at $t \approx 1.529$, 1.538 and 1.548 ps. The behavior of the frequencies during these exchanges is, in any case, completely different. While at $t \approx 1.529$ ps, the INM frequencies become quasi-degenerated, seeming to indicate that an avoided crossing is taking place, at $t \approx 1.548$ ps the INM frequencies clearly cross each other. Interestingly, in the third exchange of these INMs at $t \approx 1.538$ ps, their frequencies keep relatively apart. This kind of avoided crossing with separated frequencies are observed quite often in our MD simulations and make the convenience of using the l_{ij}^2 values instead of the frequency ordering of the INMs to identify them over time definitely clear.

The Min-Cost algorithm provides the best global one-to-one assignments of the INMs to the ENMs [48, 49]. This is clearly shown in Fig. 3 where we depict the averaged $|\boldsymbol{L}|$

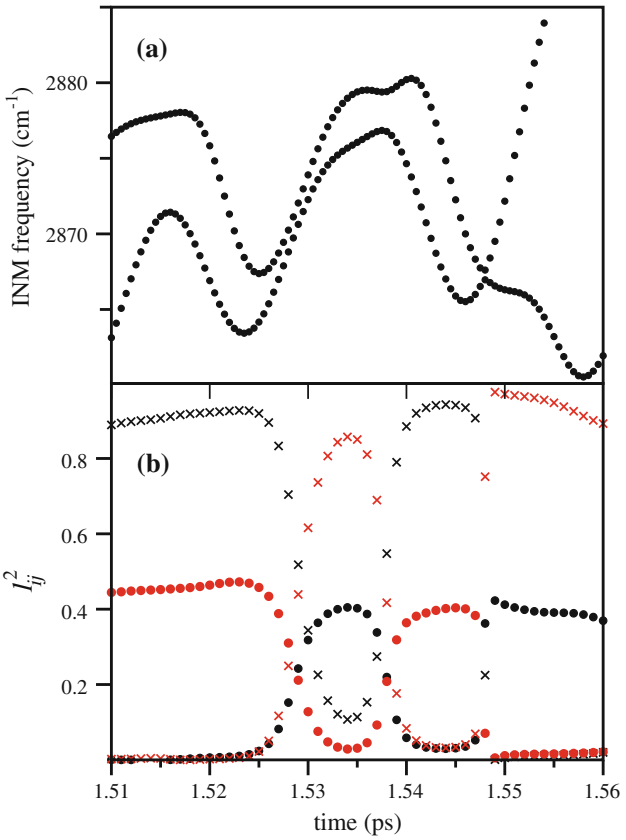

Fig. 2 **a** Evolution with time of the 25th and 26th INM frequencies of the NMAD molecule during a time interval in which they approach each other for a single trajectory. **b** Evolution with time of the corresponding values of the projection of these INMs on the 25th and 26th ENMs during the same time interval: $l_{25,25}^2$ (*black circles*), $l_{25,26}^2$ (*red circles*), $l_{26,25}^2$ (*black crosses*), and $l_{26,26}^2$ (*red crosses*)

matrix calculated directly using Eq. (7) (upper panel) and the transformed $|\boldsymbol{L}|$ matrix obtained after applying the Min-Cost algorithm (lower panel). The sizes of the bubbles in this Figure are proportional to the values of the averaged $|l_{ij}|$ matrix elements. As observed, the Min-Cost $|\boldsymbol{L}|$ matrix is much more diagonal, which indicates that the corresponding assignments are better.

As discussed above, the Min-Cost method is however not free of unphysical assignments, which occurs when two or more INMs turn out to share appreciable contributions from ENMs with quite different frequencies. In the NMAD/D_2O system, this is the case for the 1st, 2nd, 25th, and 26th INMs, which share significant contributions of the 1st, 2nd, 25th, and 26th ENMs as clearly shown in Fig. 3. To see the effect of these erroneous assignments, in Fig. 4 we show the averaged values of the INM frequencies obtained from the simulations using both the frequency ordering criterion and the Min-Cost algorithm. As observed, the 1st, 2nd, 25th, and 26th INM averaged frequencies become nearly degenerated ($\approx$1,400 cm^{-1}) when

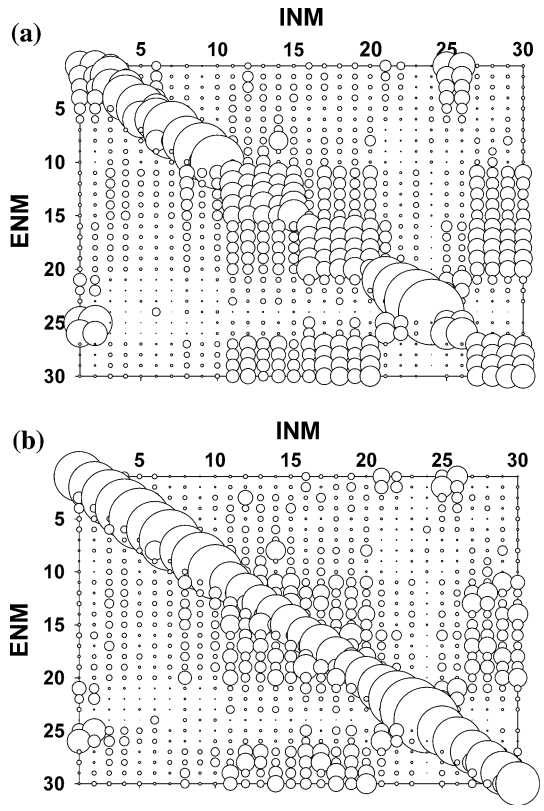

Fig. 3 Representation of the averaged $|\boldsymbol{L}|$ matrix connecting the INMs to the ENMs of the NMAD molecule in D_2O solution with the INMs assigned (**a**) by frequency ordering, and (**b**) by using the Min-Cost algorithm with $\Delta\omega$ = 400 cm^{-1}. The sizes of the bubbles are proportional to the values of the averaged $|l_{ij}|$ elements

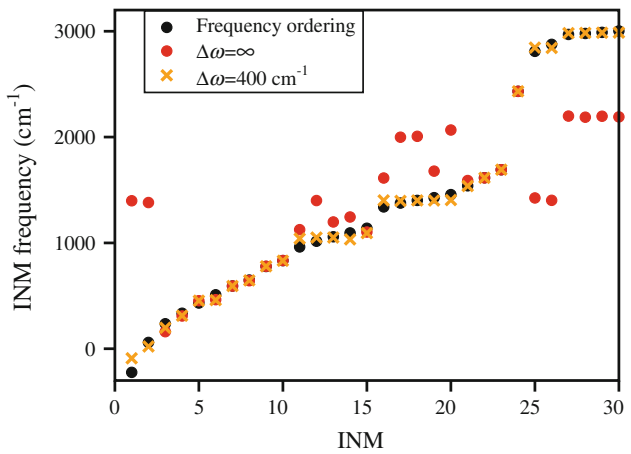

Fig. 4 Averaged values of the INM frequencies of the NMAD molecule in D_2O solution obtained from the equilibrium MD simulations using the frequency ordering criterion, and the Min-Cost algorithm with no frequency restrictions ($\Delta\omega = \infty$) and with a $\Delta\omega$ = 400 cm^{-1} frequency window

the Min-Cost algorithm is applied without restrictions due to multiple crossed assignments. A similar problem is detected in the 15th–20th and 27th–30th INMs. These

Table 2 Mean values of the highest contributions of the ENMs to the assigned INMs obtained using the frequency ordering assignment and the Min-Cost algorithm with different window sizes $\Delta\omega$ (in cm^{-1})

$\Delta\omega$	$\langle l^2_{i,f_i}\rangle$
∞	0.55
1,000	0.50
800	0.49
600	0.47
400	0.47
200	0.45
Frequency ordering	0.32

anomalies all disappear when we use the restricted Min-Cost algorithm presented in Sect. 2.2, in which only assignments to normal modes with frequencies lying in the window of width $\Delta\omega$ are considered. This is also clearly seen in Fig. 4, where we include as well the averaged values of the INM frequencies obtained from MD simulations carried out using a window of width $\Delta\omega = 400$ cm^{-1}, noting that they are closer to the meaningful values provided by frequency ordering criterion.

In order to see how the size of the frequency window influences on the efficiency of the Min-Cost algorithm, we have carried out additional INM analysis using values of $\Delta\omega$ = 200, 400, 600, 800, and 1,000 cm^{-1} and calculated the values of the l^2_{i,f_i} averaged over all the INMs for each window size which are included in Table 2. As expected, the efficiency of the restricted Min-Cost algorithm, as quantified by higher values of the l^2_{i,f_i} overlaps, increases with the window width $\Delta\omega$, with the maximum at the unrestricted Min-Cost algorithm. However, the variation of the global averaged overlaps with $\Delta\omega$ is relatively smooth, with a total change in their values of only 0.05 in the whole range of widths considered (200–1,000 cm^{-1}). From these results we consider that the 400 cm^{-1} window is the optimal one to prevent undesirable assignments without sacrificing much of the efficiency of the Min-Cost algorithm. We note also that the oscillations of the INM frequencies usually lie within this window size [46]. The improvements in the averaged l^2_{i,f_i} overlaps provided by the unrestricted ($\Delta\omega = \infty$), and restricted ($\Delta\omega$ = 400 cm^{-1}) min-Cost algorithms with respect to those given by the frequency ordering criterion are also shown in Fig. 5.

At this point we should note that, despite the improvements achieved in the INM assignments by the Min-Cost algorithm, either restricted or unrestricted, there are INMs which cannot be unambiguously assigned to a single ENM. This is clearly observed in Fig. 3b where we distinguish first a group composed of the 11th to 20th INMs, which present significant contributions from the 11th to 20th

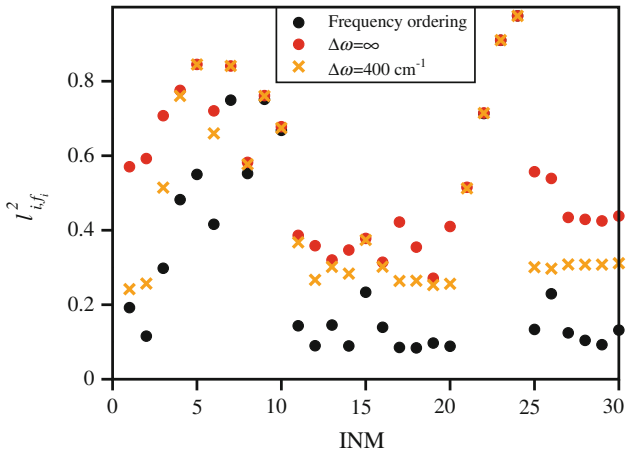

Fig. 5 Averaged values of the l^2_{i,f_i} overlaps of the NMAD INMs obtained from the equilibrium MD simulations using the frequency ordering criterion, and the Min-Cost algorithm with no frequency restrictions ($\Delta\omega = \infty$) and with a $\Delta\omega = 400$ cm^{-1} frequency window

ENMs, thus forming a well-defined block in the middle of the $\boldsymbol{L}$ matrix. This group is referred to as group a of modes [48]. The analysis of the INM frequencies of this group (see Fig. 4) shows that it is split in turn into two other well-defined groups with frequencies nearly degenerated by crossed assignments; these are the group a_1 containing the 11th to 15th INMs, which is mainly formed by the rocking methyl ENMs and a backbone ENM mode, and the group a_2 composed of the 16th to 20th INMs, which is mainly formed by the bending methyl ENMs [78]. In a similar way, Fig. 3b shows that the 25th and 26th INMs share major contributions of the 25th and 26th ENMs, which are mainly formed by the $\nu_s(CH_3)$ modes, and some minor contributions of the 1st, 2nd ENMs, which correspond to the $\tau(CH_3)$ modes [78]. These modes form the group b_1. Finally, the 27th to 30th INMs share contributions of the 27th to 30th ENMs forming the group b_2, which is made up of the more energetic stretching methyl ENMs [78]. It is also clear from Fig. 3b that there are significant couplings among the ENMs associated with the groups a_1 and a_2, and those of group b_2, resulting in a mixed composition of the corresponding INMs.

Let us consider now the usefulness of the properly identified INMs to evaluate and analyze the content of vibrational energy stored in the solute molecule. In Table 1 above, we have included the kinetic ($\langle T_i^{\mathrm{INM}}\rangle$) and harmonic potential ($\langle V_{i,\mathrm{har}}^{\mathrm{INM}}\rangle$) energies of the NMAD INMs, both in vacuo and in solution, calculated using Eqs. (15) and (16). As observed, in this case both energies for each INM agree well, in general, with the equilibrium thermodynamic value $k_BT/2 = 104.3$ cm^{-1}, in contrast to what occurs with the ENMs. The INMs therefore satisfy the virial theorem. The only exceptions here correspond to the first three INMs, for which trajectories with negative force constants λ_i which therefore give imaginary frequencies [48, 49] are found in the MD simulations. When averaged, only the vibrational frequencies of the two first of these modes remain imaginary and their values are taken as negative as is usually done [33, 35, 37]. A harmonic behavior for these three low-frequency INMs cannot therefore be expected. Our previous results [48, 49] indicate, in any case, that these modes are in fast equilibrium with the librations of the solvent, which prevents the storage of significant amounts of vibrational energy in them. We confirm then that the INMs are indeed suitable to analyze the vibrational energy content of the solute in terms of its individual normal modes contributions.

In order to investigate more deeply the relationships existing between the INMs and ENMs, we have used the ENM participation numbers P_j^{ENM} for each jth INM, which according to previous works [83, 84] are defined as follows

$$P_j^{\mathrm{ENM}} = \left(\sum_{i=1}^{N} l_{ij}^4\right)^{-1} \qquad j = 1, \ldots, N \tag{18}$$

where N is the number of ENMs of the molecule. Values of $P_j^{\mathrm{ENM}} \approx N$ correspond to extremely mixed INMs with equal contributions from every ENM, while values of $P_j^{\mathrm{ENM}} \approx 1$ correspond to INMs that are practically identical to their assigned ENMs. In Fig. 6 we show the values of P_j^{ENM} for the different INMs of the NMAD in D_2O solution, calculated using both the frequency ordering criterion and the Min-Cost algorithm with $\Delta\omega = 400$ cm^{-1}. As observed, while only two ENMs participate on average at each low-frequency INM (1st−10th INMs), for the mid-

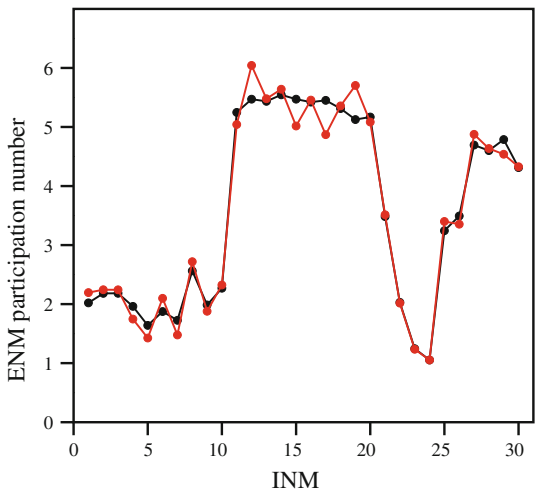

Fig. 6 ENM participation numbers P_j^{ENM} of the INMs of the NMAD molecule in D_2O solution obtained using the frequency ordering criterion (*red*) and the Min-Cost algorithm with $\Delta\omega = 400$ cm^{-1} (*black*)

range INMs belonging to the groups a_1 and a_2 the situation changes noticeably. The participation numbers rise to values $\approx 5-6$, which are slightly higher than the number 5 of INMs in each group. This small excess in the participation numbers is due to the minor contribution of the b_2 ENMs to the a_1 and a_2 groups (see Fig. 3b). The INMs that follow groups a_1 and a_2 become less mixed, with the 23rd and 24th INMs being the most localized in the spectrum with ENM participation numbers close to unity. Finally, for the high-frequency b_1 and b_2 groups, the participation numbers increase to values close to 3.5 and 4.5, respectively, since they correspond, as shown in Fig. 3b, mainly to a mixture of the ENMs associated with each group (2 and 4 respectively), plus a minor but significant contribution from groups a_1 and a_2.

Figure 6 also shows that there are no significant differences between the ENM participation numbers calculated using the frequency ordering criterion and the Min-Cost algorithm. This behavior can be explained by considering that, although the assignment by frequency ordering provides more mixed INMs than the Min-Cost algorithm, these mixings take place between INMs with similar ENM participation numbers. In order to clarify this point, we have calculated the atomic participation numbers of the normal modes defined by

$$P_j^{\mathrm{at}} = \left(\sum_{i=1}^{N_a} r_{ij}^4 \right)^{-1} \tag{19}$$

where N_a is the number of atoms in the molecule, $r_{ij}^2 = (a_{ij}^x)^2 + (a_{ij}^y)^2 + (a_{ij}^z)^2$, and a_{ij}^k $(k = x, y, z)$ are the components of the ith atom in the jth eigenvector of the Hessian matrix evaluated in the body fixed system. In this case, $P_j^{\mathrm{at}} \approx N_a$ corresponds to normal modes equally distributed through all the atoms of the molecule, and $P_j^{\mathrm{at}} \approx 1$ corresponds to normal modes involving the displacement of a single atom.

In Fig. 7, we plot the atomic participation numbers P_j^{at} calculated for the ENMs, and for the INMs obtained using frequency ordering criterion and the Min-Cost algorithm. We note first that, on average, the ENMs are only slightly more localized $\left(\langle P_j^{\mathrm{at}} \rangle_{\mathrm{ENM}} = 4.36 \pm 1.89 \right)$ than the Min-Cost INMs $\left(\langle P_j^{\mathrm{at}} \rangle_{\mathrm{INM}} = 4.61 \pm 1.41 \right)$, but the former present larger oscillations. The higher delocalization of the INMs is more pronounced in the high-frequency b_1 and b_2 groups of modes since they include important contributions from low and mid-range ENMs, as previously discussed. Also, the oscillations of the P_j^{at} values for the ENMs are comparatively more pronounced for the modes included in groups a_1 and a_2, due to the strong mixings existing in the corresponding INMs.

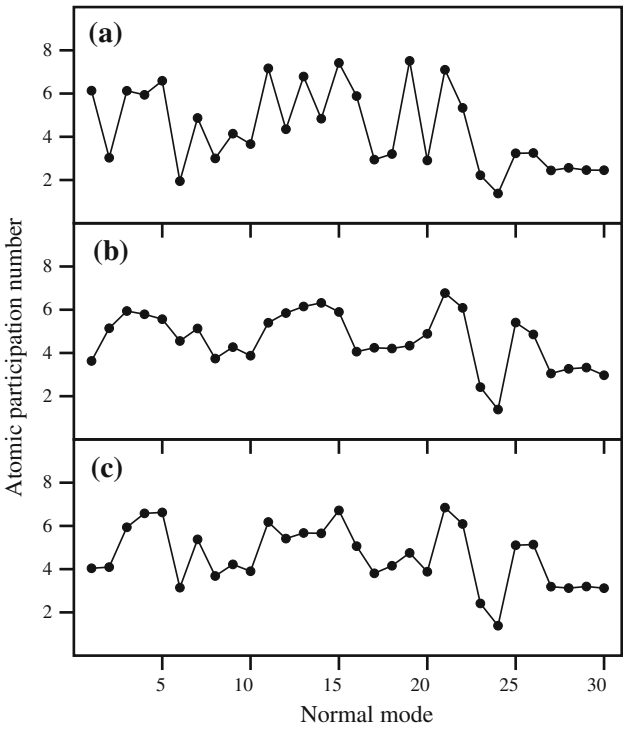

Fig. 7 Atomic participation numbers of the normal modes of the NMAD molecule in D_2O solution corresponding to **a** the ENMs, **b** the INMs assigned by frequency ordering , and **c** the INMs assigned using the Min-Cost algorithm with $\Delta\omega = 400\ \mathrm{cm}^{-1}$

When comparing the values of P_j^{at} for the INMs assigned by frequency order and by using the Min-Cost algorithm, we observe first some differences in the low-frequency regime (1st–6th INMs) indicating that INMs with different values of P_j^{at} cross, although the differences in the P_j^{at} values, while existing, remain on average close to one unit. This behavior is also observed, but attenuated, in the mid-range frequency regime. Interestingly, in the high-frequency regime, no significant differences are observed for the results obtained using both sets of INMs. Therefore, the crossings between these modes occur between states that present similar degrees of collectivity. In other words, the INMs that commonly cross involve the motion of the same atoms in the molecule. This finding, while obtained for the specific case of the NMAD molecule in D_2O solution, seems to be a general behavior to be observed in large polyatomic molecules, due to the well-known gradual increase in the INM localization with frequency [26]. That is, normal modes with similar values of P_j^{at} are likely to be close when ordered by increasing frequencies.

The development of an algorithm able to identify the INMs over time allows us to determine the time scale in which the INMs retain their identities. This can be done by computing the time-dependent INM autocorrelation function of each eigenvector $Q_i^{\mathrm{INM}}(t)$, which is given by

$$C_i^{\mathrm{INM}}(\Delta) = \langle Q_i^{\mathrm{INM}}(t) Q_i^{\mathrm{INM}}(t+\Delta) \rangle = \frac{1}{T} \int_0^T Q_i^{\mathrm{INM}}(t) Q_i^{\mathrm{INM}}(t+\Delta) \mathrm{dt} \quad (20)$$

where the overlap is

$$Q_i^{\mathrm{INM}}(t) Q_i^{\mathrm{INM}}(t+\Delta) = \sum_{k=1}^{N} l_{k,i}(t) l_{k,i}(t+\Delta) \quad (21)$$

Since the INMs are obtained by numerical diagonalization of the Hessian matrix of the ENMs (see Eq. (7)), their signs may change on account of an arbitrary choice of the phase, and this complicates the evaluation of the INM autocorrelation function. To address this problem, we have made the definition of the INMs uniform by taking the l_{i,f_i} elements to be positive. Thus, if after diagonalization of the Hessian matrix and application of the Min-Cost algorithm, the value of l_{i,f_i} is negative, we change the sign of all elements in the f_ith column.

In order to facilitate the comparison of the autocorrelation functions for the different INMs, we have used the normalized autocorrelation function, defined as

$$C_{i,\mathrm{norm}}^{\mathrm{INM}}(\Delta) = \frac{C_i^{\mathrm{INM}}(\Delta) - C_{i,\mathrm{eq}}^{\mathrm{INM}}}{C_i^{\mathrm{INM}}(0) - C_{i,\mathrm{eq}}^{\mathrm{INM}}} \quad (22)$$

where $C_i^{\mathrm{INM}}(0) = 1$ and $C_{i,\mathrm{eq}}^{\mathrm{INM}}$ is the asymptotic value of the autocorrelation function for the ith INM. We have found that the asymptotic value $C_{i,\mathrm{eq}}^{\mathrm{INM}}$ is equal to the mean value of the l_{i,f_i}^2 contributions of the ENMs to the assigned INMs, since all the remaining contributions tend to cancel out because they turn out eventually to have equally likely opposite signs at long times.

In Fig. 8 we show the normalized autocorrelation functions $C_{i,\mathrm{norm}}^{\mathrm{INM}}(\Delta)$ of the INMs of the NMAD molecule in D_2O solution, arranged in groups with similar fluctuation patterns. According to Fig. 3, these groups correspond to

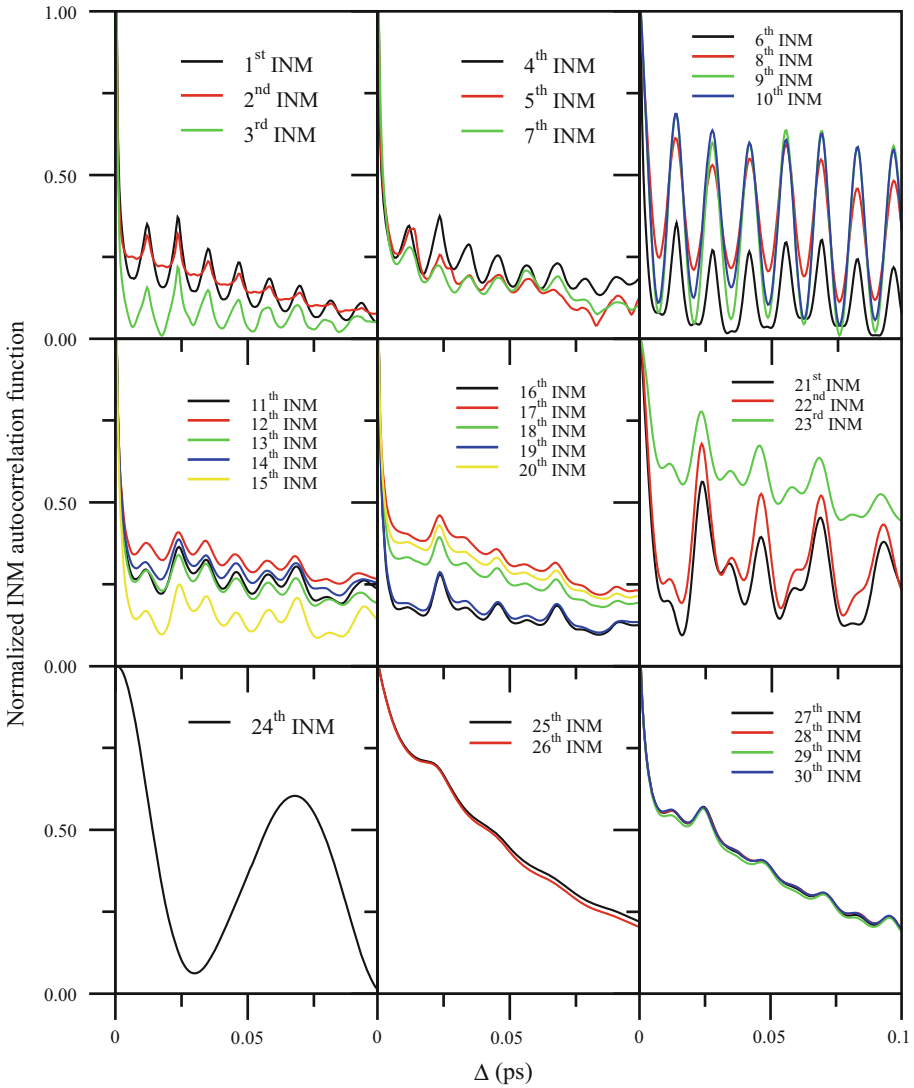

Fig. 8 Normalized autocorrelation functions, $C_{i,\mathrm{norm}}^{\mathrm{INM}}(\Delta)$ of the INMs of NMAD in D_2O solution

INMs modes which mix with each other over time. It is interesting to note the marked oscillating character that the autocorrelation functions of the 1st–23rd INMs have, with periods of about 10–15 fs, in contrast with the much less evident oscillations presented by the modes of the high-frequency groups b_1 and b_2. In the middle we also have the particular case of the 24th INM. This is the amide A mode and, as shown in Fig. 5, is the purest one, with the highest averaged l^2_{i,f_i} contribution in the spectrum. As observed in Fig. 8, this mode also mixes with other INMs so that its autocorrelation function oscillates with a period longer than those of the other modes and closer to the oscillation period of its own averaged vibrational frequency.

The oscillations in the autocorrelation functions of the INMs make it difficult to obtain relaxation times that characterize the loss of identity of the modes in a simple way. Some trends are observed however in Fig. 8. Most of the low and mid-range INMs undergo an initial fast decay in the time scale of femtoseconds followed by a much slower relaxation while the 8th, 9th, and 10th INMs show a pronounced oscillatory slower decay. Meanwhile, the decay of the autocorrelation function of the high-frequency INMs slows down from the beginning, with INM lifetimes in the range of 25–50 fs.

4 Summary and conclusions

In this paper, we have developed and discussed in depth a new method to analyze the intramolecular vibrational dynamics of polyatomic molecules in solution based on the use of the instantaneous normal modes of the solute molecule. To illustrate the method, we have carried out equilibrium MD simulations of the vibrational dynamics of the NMAD molecule in liquid D_2O.

We have shown first that the vibrational energy of the solute molecule cannot be accurately expressed as the sum of the individual harmonic contributions of the equilibrium normal modes. The alternative is to use the INMs, which requires of an efficient method to assign them in order to track their identities as the whole system evolves with time. The simple identification of the INMs by frequency ordering is not useful in this respect due to the multiple crossings and mixings that the modes undergo over time. We therefore propose a novel identification method of the INMs based on the use of the ENMs as templates to establish a one-to-one correspondence between both sets of modes through the highest values of their overlaps. The maximum overlaps between both sets of modes are found by using the so-called Min-Cost algorithm, properly adapted to the maximization of the trace of the overlap matrix. In addition, we impose restrictions on the Min-Cost algorithm in order to avoid unphysical interchanges between two or more INMs which share contributions of ENMs with very different vibrational frequencies. These restrictions consist specifically of applying the Min-Cost algorithm for each INMs in a frequency window of width $\Delta\omega$ centered at the value of ENM vibrational frequency ω^e_i.

By using the INMs-based method proposed to study the equilibrium vibrational dynamics of the NMAD/$D_2O_{(l)}$ system, we have shown first that the INMs of the NMAD molecule can indeed be used to account for the vibrational energy content stored in each individual mode and thus to monitor the evolution with time of the vibrational energy of the solute molecule. Second, we have demonstrated that the Min-Cost algorithm improves the assignments of the INMs of the NMAD molecule versus the simple frequency ordering criterion and that the restricted Min-Cost algorithm refines the identification of the INMs further by avoiding unphysical assignments. For the NMAD/$D_2O_{(l)}$ system, a window of width $\Delta\omega = 400$ cm^{-1} was found to be optimal to prevent undesirable assignments without sacrificing much of the efficiency of the Min-Cost method. Third, it has been shown that some groups of INMs remain quite mixed throughout the whole dynamics of the system, so they can be perfectly identified as well-defined groups of modes which interchange vibrational energy with the rest of INMs. Participation numbers have been used in this case to analyze the composition and nature of these groups. Finally, we have calculated the autocorrelation functions of the INMs, which tend asymptotically to the mean values of the highest overlaps with the ENMs. The analysis of the autocorrelation functions reveals that the INMs have short lifetimes and that they can be gathered in groups with similar fluctuation patterns.

Acknowledgments This work was partially supported by the Ministerio de Educación y Ciencia of Spain under Project CTQ2007-66528/BQU and CONSOLIDER CSD2009-00038, by the Fundación Séneca del Centro de Coordinación de la Investigación de la Región de Murcia under Project 08735/PI/08, by the Universidad Nacional de Quilmes, and by CONICET. M.A.S. and M.H.F. both acknowledge fellowships provided by the Ministerio de Educación y Ciencia of Spain, and A.K. acknowledges a fellowship provided by CONICET.

References

1. Hill JR, Ziegler CJ, Suslick KS, Dlott DD, Rella CW, Fayer MD (1996) Tuning the vibrational relaxation of co bound to heme and metalloporphyrin complexes. J Phys Chem 100:18023–18032
2. Hamm P, Lim MH, Hochstrasser RM (1998) Structure of the amide i band of peptides measured by femtosecond nonlinear-infrared spectroscopy. J Phys Chem B 102 (31):6123–6138
3. Peterson KA, Rella CW, Engholm JR, Schwettman HA (1999) Ultrafast vibrational dynamics of the myoglobin amide i band. J Phys Chem B 103(3):557–561
4. Dlott DD (2001) Vibrational energy redistribution in polyatomic liquids: 3d infrared-raman spectroscopy. Chem Phys 266:149

5. Iwaki L, Dlott DD (2001) Vibrational energy transfer in condensed phases. In: Moore JH, Spencer ND (eds) Encyclopedia of chemical physics and physical chemistry. IOP Publishing Ltd, Bristol, p 2717
6. Fayer MD (2001a) Fast protein dynamics probed with infrared vibrational echo experiments. Annu Rev Phys Chem 52:315
7. Fayer MD (2001b) Ultrafast infrared and Raman spectroscopy. Marcel Dekker Inc, New York
8. Cremeens ME, Fujisaki H, Zhang Y, Zimmermann J, Sagle LB, MAtsuda S, Dawson PE, Straub JE, Romesberg FE (2006) Efforts toward developing direct probes of protein dynamics. J Am Chem Soc 128:6028–6029
9. Shigeto S, Dlott DD (2007) Vibrational relaxation of an amino acid in aqueous solution. Chem Phys Lett 447:134–139
10. Wang ZH, Carter JA, Lagutchev A, Koh YK, Seong N-H, Cahill DG, Dlott DD (2007) Ultrafast flash thermal conductance of molecular chains. Science 317:787
11. Shigeto S, Pang Y, Fang Y, Dlott DD (2008) Vibrational relaxation of normal and deuterated liquid nitromethane. J Phys Chem B 112:232–241
12. Schade M, Moretto A, Crisma M, Toniolo C, Hamm P (2009) Vibrational energy trasnport in pepetide helices after excitation of c-d modes in leu-d_{10}. J Phys Chem A 113:13393–13397
13. Fang Y, Shigeto S, Seong N, Dlott D (2009) Vibrational energy dynamics of glycine, n-methylacetamide, and benzoate anion in aqueous (d2o) solution. J Phys Chem A 113(1):75–84
14. Nguyen PH, Stock G (2003) Nonequilibrium molecular-dynamics study of the vibrational energy relaxation of peptides in water. J Chem Phys 119(21):11350–11358
15. Frauenfelder H, Bishop AR, Garcia A, Perelson A, Schuster P, Sherrington D, Swart PJ (1997) Landscape paradigms in physics and biology: Concepts, structures, and dynamics. North-Holand, Amsterdam
16. Frauenfelder H, McMahon BH, Austin RH, Chu K, Groves JT (2001) The role of structure, energy landscape, dynamics, and allostery in the enzymatic function of myoglobin. Proc Natl Acad Sci USA 98:2370–2374
17. Frauenfelder H, McMahon BH, Fenimore PW (2003) Myoglobin: The hydrogen atom of biology and a paradigm of complexity. Proc Natl Acad Sci 100:8615–8617
18. Lubchenko V, Wolynes PG, Frauenfelder H (2005) Mosaic energy landscapes of liquids and the control of protein conformational dynamics by glass-forming solvents. J Phys Chem B 109:7488–7499
19. Moritsugu K, Miyashita O, Kidera A (2000) Vibrational energy transfer in a protein molecule. Phys Rev Lett 85:3970–3973
20. Roitberg A, Gerber BB, Ratner MA (1997) A vibrational eigenfunction of a protein: Anharmonic coupled-mode ground and fundamental excited states of bpti. J Phys Chem B 101:1700–1706
21. Hayward S, Kitao A, Go N (1994) Harmonic and anharmonic aspects in the dynamics of bpti: A normal mode analysis and principal component analysis. Protein Sci 3:936–943
22. Go N, Noguti T, Nishikawa T (1983) Dynamics of a small globular protein in terms of low-frequency vibrational-modes. Proc Natl Acad Sci USA 80:3696
23. Hayward S, Kitao A, Go N (1995) Harmonicity and anharmonicity in protein dynamics: A normal mode analysis and principal component analysis. Proteins 23:177–186
24. Ohmine I, Tanaka H (1990) Potential energy surfaces for water dynamics. II. Vibrational mode excitations, mixing and relaxations. J Chem Phys 93:8138–8147
25. Ohmine I, Tanaka H (1993) Fluctuation, relaxations, and hydration in liquid water. hydrogen-bond rearrangement dynamics. Chem Rev 93:2545–2566
26. Sagnella DE, Straub JE (1999) A study of vibrational relaxation of b-state carbon monoxide in the heme pocket of photolyzed carboxymyoglobin. Biophys J 77:70–84
27. Rao F, Karplus M (2010) Protein dynamics investigated by inherent structure analysis. Proc Natl Acad Sci USA 107:9152–9157
28. Elber R, Karplus M (1987) Multiple conformational states of proteins: A molecular dynamics analysis of myoglobin. Science 235:318
29. Fujisaki H, Stock G (2008) Dynamic treatment of vibrational energy relaxation in a heterogeneous and fluctuating environment. J Chem Phys 129(13):134110
30. Levy RM, Perahia D, Karplus M (1982) Molecular-dynamics of an alpha-helical polypeptide-temperature-dependence and deviation from harmonic behavior. Proc Natl Acad Sci USA 79:1346–1350
31. Karplus M, Kushick J (1981) Method for estimating the configurational entropy of macromolecules. Macromolecules 14:325–332
32. Levy RM, Karplus M, Kushick J, Perahia D (1984) Evaluation of the configurational entropy for proteins—Application to molecular-dynamics simulations of an alpha-helix. Macromolecules 17:1370–1374
33. Buchner M, Ladanyi B, Stratt RM (1992) The short-time dynamics of molecular liquids. Instantaneous-normal-mode theory. J Chem Phys 97:8522–8535
34. Goodyear G, Stratt RM (1997) The short-time intramolecular dynamics of solutes in liquids. 2. Vibrational population relaxation. J Chem Phys 107:3098–3120
35. Keyes T (1997) Instantaneous normal mode approach to liquid state dynamics. J Phys Chem A 101:2921–2930
36. David EF, Stratt RM (1998) The anharmonic features of the short-time dynamics of fluids: The time evolution and mixing of instantaneous normal modes. J Chem Phys 109:1375–1390
37. Stratt RM (2001) The molecular mechanism behind the vibrational population relaxation of small molecules in liquids. In: Fayer MD (eds) Ultrafast infrared and Raman spectroscopy. Marcel Dekker Inc, New York, pp. 149–190
38. Garberoglio G, Vallauri R (2002) Instantaneous normal mode analysis of short-time dynamics in hydrogen-bonded liquids. Physica A 314:492–500
39. Kramer N, Buchner M, Dorfmuller T (1998) Normal mode dynamics in simple liquids. J Chem Phys 109:1912–1919
40. Moore PB, Ji XD, Ahlborn H, Space B (1998) An instantaneous normal mode theory of condensed phase absortion: The vibrational spectrum of condensed cs_2 from bpiling to freezing. Chem Phys Lett 296:259–265
41. Ahlborn H, Ji XD, Space B, Moore PB (1999) A combined instantaneous normal mode and time correlation function description of the infrarred vibrational spectrum of ambient water. J Chem Phys 111:10622–10632
42. Ji XD, Alhborn H, Space B, Moore PB, Zhou Y, Constantine S, Ziegler LD (2000) A combined instantaneous normal mode and time correlation function description of the optical Kerr effect and Raman spectroscopy of liquid cs_2. J Chem Phys 112:4186–4192
43. Perry A, Ahlborn H, Space B, Moore PB (2003) A combined time correlation function and instantaneous normal mode study of the sum frequency generation spectroscopy of the water/vapor interface. J Chem Phys 118:8411–8419
44. Deng YQ, Ladanyi BM, Stratt RM (2002) High-frequency vibrational energy relaxation in liquids: The foundations of instantaneous-pair theory and some generalizations. J Chem Phys 117:10752–10767
45. Bu L, Straub JE (2003) Vibrational frequency shifts and relaxation rates for a selected vibrational mode in cytochrome c. Biophys J 85:1429–1439

46. Fujisaki H, Yagi K, Straub JE, Stock G (2009) Quantum and classical vibrational relaxation dynamics of n-methylacetamide on ab initio potential energy surfaces. Int J Quant Chem 109:2047–2057
47. Schulz R, Krishnana M, Daidone I, Smith JC (2009) Instantaneous normal modes and the protein glass transition. Biophys J 96:476–484
48. Bastida A, Soler MA, Zúñiga J, Requena A, Kalstein A, Fernandez-Alberti S (2010) Instantaneous normal modes, resonances and assignments in the vibrational relaxation of the amide i mode of n-methylacetamide-d in aqueous (d_2o) solution. J Chem Phys 132:224501
49. Bastida A, Soler MA, Zúñiga J, Requena A, Fernández-Alberti S, Kalstein A (in press) Molecular dynamics simulations and instantaneous normal mode analysis of the vibrational relaxation of the C–H stretching modes of *n*-methylacetamide-d in liquid deuterated water. J Phys Chem A (in press)
50. Cho M, Fleming GR, Saito S, Ohmine I, Stratt RM (1994) Instantaneous normal-mode analysis of liquid water. J Chem Phys 100:6672–6683
51. Ladanyi BM, Klein S (1996) Contributions of rotation and translation to polarizability anisotropy and solvation dynamics in acetonitrile. J Chem Phys 105:1552–1561
52. Stratt RM, Cho M (1994) The short-time dynamics of solvation. J Chem Phys 100:6700–6708
53. Kalbfleisch TS, Ziegler LD, Keyes T (1996) An instantaneous normal mode analysis of solvation: Methyl iodide in high pressure gases. J Chem Phys 105:7034–7046
54. Egorov SA, Stephens MD, Skinner JL (1996) Absorption line shapes and solvation dynamics of ch3i in supercritical ar. J Chem Phys 107:10485–10491
55. Ladanyi BM, Stratt RM (1995) Short-time dynamics of solvation—Linear solvation theory for polar-solvents. J Phys Chem 99:2502–2511
56. Ladanyi BM, Stratt RM (1996) Short-time dynamics of solvation: Relationship between polar and nonpolar solvation. J Phys Chem 100:1266–1282
57. Woutersen S, Mu Y, Stock G, Hamm P (2001) Subpicosecond conformational dynamics of small peptides probed by two-dimensional vibrational spectroscopy. Proc Natl Acad Sci USA 98:11254
58. Zanni MT, Asplund MC, Hochstrasser RM (2001) Two-dimensional heterodyned and stimulated infrared photon echoes of n-methylacetamide-d. J Chem Phys 114:4579–4590
59. Woutersen S, Pfister R, Hamm P, Mu Y, Kosov DS, Stock G (2002) Peptide conformational heterogeneity revealed from nonlinear vibrational spectroscopy and molecular-dynamics simualtions. J Chem Phys 117:6833–6840
60. Rubtsov IV, Wang J, Hochstrasser RM (2003) Vibrational coupling between amide-i and amide-a modes revealed by femtosecond two color infrared spectroscopy. J Phys Chem A 107:3384–3396
61. DeCamp MF, DeFlores L, McCracken JM, Tokmakoff A, Kwac K, Cho M (2005) Amide i vibrational dynamics of n-methylacetamide in polar solvents: The role of electrostatic interactions. J Phys Chem B 109(21):11016–11026
62. DeFlores LP, Ganim Z, Ackley SF, Chung HS, Tokmakoff A (2006) The anharmonic vibrational potential and relaxation pathways of the amide I and II modes of n-methylacetamide. J Phys Chem B 110(38):18973–18980
63. Gregurick SK, Chaban GM, Gerber RB (2002) Ab initio and improved empirical potentials for the calculation of the anharmonic vibrational states and intramolecular mode coupling of n-methylacetamide. J Phys Chem A 106(37):8696–8707
64. Kwac K, Cho M (2003) Molecualr dynamics simualtion study of n-methylacetamide in water. I. Amide I mode frequency fluctuation. J Chem Phys 119:2247–2255
65. Schmidt JR, Corcelli SA, Skinner JL (2004) Ultrafast vibrational spectroscopy of water and aqueus n-methylacetamide. Comparison of different electronic structure/molecular dynamics approaches. J Chem Phys 121:8887–8896
66. Hayashi T, Zhuang W, Mukamel S (2005) Electrostatic DFT map for the complete vibrational amide band of NMA. J Phys Chem A 109:9747–9759
67. Fujisaki H, Zhang Y, Straub JE (2006) Time-dependent perturbation theory for vibrational energy relaxation and dephasing in peptides and proteins. J Chem Phys 124(14):144910
68. Fujisaki H, Yagi K, Hirao K, Straub JE (2007) Quantum dynamics of n-methylacetamide studied by the vibrational configuration interaction method. Chem Phys Lett 443:6–11
69. Goodyear G, Stratt RM (1996) The short time intramolecular dynamics of solutes in liquids. I. An instantaneous normal mode theory for friction. J Chem Phys 105:10050–10071
70. Ladanyi BM, Stratt RM (1998) The short-time dynamics of vibrational relaxation in molecular liquids. J Phys Chem A 102:1068–1082
71. Carpaneto G, Martello S, Toth P (1988) Algorithms and codes for the assigment problem. Ann Oper Res 13:193–223
72. Nakamura M, Tamura K, Murakami S (1995) Isotope effects on thermodynamic properties: Mixtures of $x(d_2o$ or $h_2o) + (1 - x)$ ch_3cn at 298.15 k. Thermochim Acta 253:127–136
73. Cornell WD, Cieplak P, Bayly CI, Gould IR, Merz KM Jr, Ferguson DM, Spellmeyer DC, Fox T, Caldwell JW, Kollman PA (1995) A second generation force field for the simulation of proteins, nucleic acids, and organic molecules. J Am Chem Soc 117:5179–5197
74. MacKerell AD Jr, Bashford D, Bellott M, Dunbrack RL Jr, Evanseck JD, Field MJ, Fischer S, Gao J, Guo H, Ha S, Joseph-McCarthy D, Kuchnir L, Kuczera K, Lau FTK, Mattos C, Michnick S, Ngo T, Nguyen DT, Prodhom B, Reiher WE III, Roux B, Schlenkrich M, Smith JC, Stote R, Straub J, Watanabe M, Wiórkiewicz-Kuczera J, Yin D, Karplus M (1998) All-atom empirical potential for molecular modeling and dynamics studies of proteins. J Phys Chem B 102(18):3586–3616
75. Pappu RV, Hart RK, Ponder JW (1998) Analysis and application of potential energy smoothing and search methods for global optimization. J Phys Chem B 102:9725–9742
76. Allen MP, Tildesley DJ (1987) Computer simulation of liquids. Oxford Science Publications, Oxford
77. Svanberg M (1997) An improved leap-frog rotational algorithm. Mol Phys 92:1085
78. Rey-Lafon M, Forel MT, Garrigou-Lagrange C (1973) Discussion des modes normaux des groupements amides cis et trans partir des champs de force du δ-valrolactame et du n-methylacetamide. Spectr Acta 29A:471–486
79. Ataka S, Takeuchi H, Tasumi M (1984) Infrared studies of the less stable cis form of n-methylformamide and n-methylacetamide in low-temperature nitrogen matrices and vibrational analyses of the trans and cis forms of these molecules. J Mol Struct 113:147–160
80. Berendsen HJC, Postma JPM, van Gunsteren WF, DiNola A, Haak JR (1984) Molecular-dynamics with coupling to an external bath. J Chem Phys 81:3684
81. Raff LM (1988) Projection methods for obtaining intramolecular energy-transfer rates from classical trajectory results—Application to 1,2-difluoroethane. J Chem Phys 89(9):5680–5691
82. Kabadi VN, Rice BM (2004) Molecular dynamics simualtions of normal mode vibrational energy transfer in liquid nitromethane. J Phys Chem A 108:532–540
83. Bell RJ, Dean P, Hibbins-Butler C (1970) localization of normal modes in vitreous silica, germania and beryllium fluoride. J Phys C: Solid St Phys 3:2111–2118
84. Taraskin SN, Elliott SR (1999) Anharmonicity and localization of atomic vibrations in vitreous silica. Phys Rev B 59:8572–8585